Electro-Optical Navigation for Aircraft

P. K. A. MENON
Georgia Institute of Technology

G. B. CHATTERJI

B. SRIDHAR, Senior Member, IEEE
NASA Ames Research Center

Low altitude flight is extremely demanding on the rotorcraft pilots. This fact has motivated the research in automating various components of low altitude rotorcraft flight operations. Concurrent with the development of guidance laws, efforts are underway to develop systems for locating the terrain and the obstacles using inputs from passive electro-optical sensors such as TV cameras and infrared imagers. A passive obstacle location algorithm that uses image sequences from cameras undergoing translational and rotational motion is developed. The algorithm is in a general form and can operate in multicamera imaging environments. Performance results using an image sequence from an airborne camera are given.

Manuscript received September 22, 1991; revised August 3, 1992.

IEEE Log No. T-AES/29/3/07996.

The work of P. K. A. Menon was supported by NASA under Cooperative Agreement NCC2-575.

Authors' current addresses: P. K. A. Menon, Optimal Synthesis, 908 E. Meadow Dr., Palo Alto, CA 94303; G. B. Chatterji, Sterling Software, Inc., 1121 San Antonio Rd., Palo Alto, CA 94303; B. Sridhar, FSN Branch, M.S. 210-9, NASA Ames Research Center, Moffett Field, CA 94035.

INTRODUCTION

Low altitude flight mode is one in which a rotorcraft flies close to the terrain, with an altitude clearance of less than 50 ft, while avoiding various obstacles on the way under all weather conditions. This flight regime is extremely taxing on the rotorcraft pilots who have to carry out many other duties in addition to flying the aircraft. These factors have motivated the research in automating the low altitude flight regime [1–3].

The task of locating various obstacles within the field-of-view has emerged as the central problem in the development of pilot aids for low altitude flight. Use of active sensors such as radar or laser rangers are not desirable due to their significant power requirements and the difficulty in conducting covert missions with such devices on-board. This issue has driven the research in developing passive obstacle location schemes using conventional TV and infrared imaging devices.

Several approaches to the image-based obstacle location problem have emerged in recent years [4–9]. Specifically, [4] has discussed the development of a recursive obstacle location scheme for low altitude helicopter flight. In that approach, various features of interest in an image sequence such as regions of high contrast are used to determine the location of various objects within the field-of-view. Techniques such as these are termed as *feature-based* to distinguish them from techniques that do not explicitly use any object features for determining their location. Image-based obstacle location algorithms that do not explicitly employ features are termed *field-based* approaches. Various aspects of a field-based algorithm are discussed in [7–9].

In the present work, the field-based obstacle location scheme discussed in [7–9] is extended to permit the inclusion of rotational and translational motion of the imaging devices and the rotorcraft. While such an extension is nontrivial, this aspect needs to be addressed before an operational system can be synthesized.

VISION-BASED OBSTACLE LOCATION

Passive obstacle location methods using electro-optical sensors have their basis in the fact that the images obtained from sensors mounted on a moving vehicle will exhibit irradiance changes at each pixel. Relative location of various objects, vehicle motion parameters, relative location of the imaging devices, the scene surface reflectance, and the location of illumination sources all influence this irradiance change. If the surface reflectance and the illumination are assumed to remain constant during the imaging process, then the observed image irradiance changes at each pixel are entirely due to the relative location

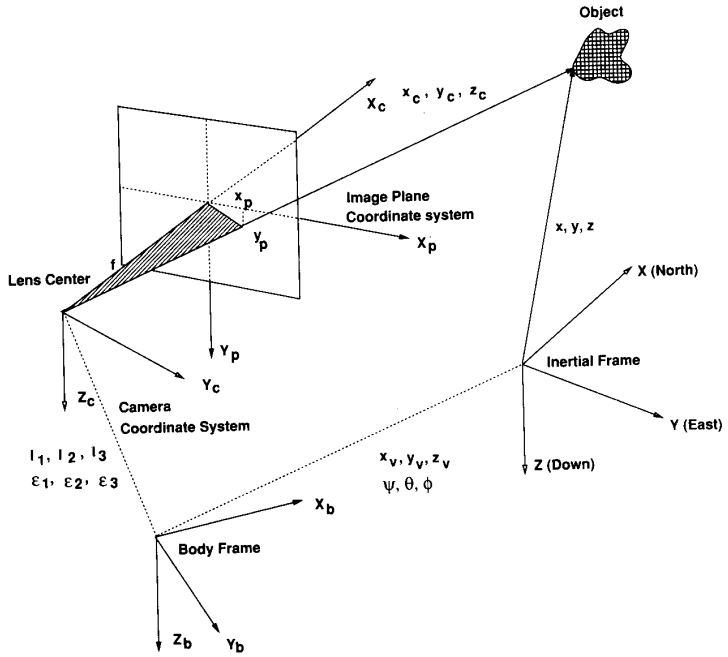

Fig. 1. Coordinate system.

of various objects within the field-of-view and the vehicle motion parameters. Additionally, if all the objects within the field-of-view are assumed fixed with respect to an inertial frame, then the irradiance change at each pixel location can be directly related to the location of these objects. In this case, if the vehicle motion parameters and the imaging device constants are known, it is possible to determine the location of various points within the field-of-view.

Image-based obstacle location algorithms operate on the basis of the *correspondence hypothesis*. The central idea here is to establish the correspondence between various objects in a pair of images and to measure the displacement of these objects on the image plane. The measured displacement or the *disparity* can then be employed together with the perspective projection geometry for computing the location of various objects within the field-of-view.

In order further to crystallize these ideas, consider the various coordinate systems illustrated in Fig. 1. The first of these is the image plane coordinate system with the major axis of the image plane being designated as the X_p axis and the minor axis being labelled the Y_p axis. The origin of this image plane coordinate system is located at the center of the aperture. In this coordinate system, an image may be defined as an irradiance distribution $E(x_p,y_p)$, with E being the irradiance specified on a gray scale at a point x_p,y_p on the image plane. Next consider the camera coordinate system X_c, Y_c, Z_c with the X_c axis passing through the origin of the image-plane coordinate system, and the axes Y_c, Z_c being parallel to the image plane coordinate system. The origin of the camera coordinate system is at the lens center, located one focal length f behind the image plane X_p, Y_p. Such an arrangement of the camera coordinate system is routinely employed in image processing work to avoid having to deal with inverted images.

The origin of the camera coordinate system is assumed to be located at a point l_1, l_2, l_3 with respect to the body axis, and oriented by three angles ϵ_1, ϵ_2, ϵ_3 about the Z_c, Y_c, and X_c axes, respectively. The vehicle body axis system is defined using the standard flight dynamics convention, viz., the X_b axis pointing along the nose of the rotorcraft, Y_b axis along the starboard direction, and the Z_b axis completing the right-handed triad. The body axis system may be related to an inertial frame X, Y, Z through yaw, pitch, roll Euler angles ψ, θ, ϕ and the three translational components x_v, y_v, z_v. The definition of the inertial frame follows the standard flight dynamics convention with the X axis pointing toward north, the Y axis pointing toward east, and the Z axis pointed in the direction of local gravity vector.

A point x_p, y_p corresponding to the object in the image plane is related to its location with respect to the inertial frame x, y, z through various translations and rotations of the vehicle body frame and the camera frame, together with the perspective projection.

Let $E_1(x_p,y_p)$ and $E_2(x_p,y_p)$ be two different views of a sample scene. Assuming that these two images contain all the objects of interest and that to a large degree, the perceived irradiance of the scene has remained invariant during the imaging process, the

correspondence hypothesis can be expressed as

$$E_1(x_p, y_p) = E_2(x_p + \Delta x_{p2}, y_p + \Delta y_{p2}) \quad (1)$$

$$E_2(x_p, y_p) = E_1(x_p - \Delta x_{p1}, y_p - \Delta y_{p1}). \quad (2)$$

Here, Δx_{p1}, Δy_{p1}, Δx_{p2}, Δy_{p2} are the disparities between the corresponding points in the two images defined at every point on the image plane. Assuming that the same object is being observed at the pixel location x_p, y_p in these two images, one has that $\Delta x_{p1} = -\Delta x_{p2}$, $\Delta y_{p1} = -\Delta y_{p2}$.

It is important to stress that the correspondence hypothesis expressed in (1) and (2) should be interpreted in a limited sense because it does not account for various occlusions that can arise during the imaging process. These occlusions arise due to the viewing angle and the camera aperture dimensions. Note that equations such as (1) and (2) can be written for any number of images, provided that the objects of interest appear in all the images. Various methods for satisfying the correspondence hypothesis have been discussed in the literature [4–10]. In the present research, the correspondence hypothesis is approximated by first expanding the expressions (1) and (2) in a Taylor series and then truncating them based on the acceptable computational complexity. Such an expansion treats disparities Δx_p, Δy_p as perturbations about the specified pixel locations. Clearly, the error in such an approximation depends on the number of terms included in the Taylor series.

In all that follows, a bold face lower case letter denotes a vector, while a bold face upper case letter denotes a matrix. A superscript T is used to denote the vector-matrix transpose operation. Define the disparity vector $\mathbf{d}$, the irradiance gradient vector $\mathbf{g}$, and the irradiance Hessian matrix $\mathbf{H}$ as

$$\mathbf{d} = \begin{bmatrix} \Delta x_p \\ \Delta y_p \end{bmatrix}; \qquad \mathbf{g} = \begin{bmatrix} \partial E/\partial x_p \\ \partial E/\partial y_p \end{bmatrix}$$
$$\mathbf{H} = \begin{bmatrix} \partial^2 E/\partial x_p^2 & \partial^2 E/\partial x_p \partial y_p \\ \partial^2 E/\partial y_p \partial x_p & \partial^2 E/\partial y_p^2 \end{bmatrix}. \quad (3)$$

Equations (1) and (2) can now be expanded using a two-dimensional Taylor series to yield

$$E_1 - E_2 = \mathbf{g}_2^{\mathrm{T}}\mathbf{d} + \tfrac{1}{2}\mathbf{d}^{\mathrm{T}}\mathbf{H}_2\mathbf{d} + \cdots. \quad (4)$$

Similarly,

$$E_2 - E_1 = -\mathbf{g}_1^{\mathrm{T}}\mathbf{d} + \tfrac{1}{2}\mathbf{d}^{\mathrm{T}}\mathbf{H}_1\mathbf{d} - \cdots. \quad (5)$$

Expressions (4) and (5) relate the irradiance spatial partial derivatives to the irradiance change and the image disparities at every pixel. It is awkward to express the terms beyond second-order in (4) and (5) using the vector-matrix notation because they contain tensors.

In the special case where the disparities Δx_p, Δy_p arise from the vehicle motion resulting in apparent image velocities, the equations (4) and (5), with the first term on the right-hand side, become the *optical flow constraint equation* [10]. In this case, the apparent image velocity components are called the optical flow velocities. This characterization is avoided here because the disparities Δx_p, Δy_p may arise from other sources also, stereo camera arrangement being an example. By adopting the point-of-view proposed in the foregoing, (4) and (5) may be used for temporal image sequences from a single camera motion sequence as well as simultaneous images obtained from several cameras.

Adding and subtracting the expressions (4) and (5) results in

$$E_1 - E_2 = \tfrac{1}{2}[\mathbf{g}_1 + \mathbf{g}_2]^{\mathrm{T}}\mathbf{d} + \tfrac{1}{4}\mathbf{d}^{\mathrm{T}}[\mathbf{H}_2 - \mathbf{H}_1]\mathbf{d} + \cdots \quad (6)$$

$$0 = [\mathbf{g}_2 - \mathbf{g}_1]^{\mathrm{T}}\mathbf{d} + \tfrac{1}{2}\mathbf{d}^{\mathrm{T}}[\mathbf{H}_1 + \mathbf{H}_2]\mathbf{d} + \cdots. \quad (7)$$

Next, as in [8], equation (6) is used for obstacle location, while the expression (7) is used for computing the truncation error in the Taylor series approximation. The components of the disparity vector Δx_p, Δy_p can now be related to the vehicle motion parameters and the location of various objects in the field-of-view.

Let x_c, y_c, z_c be the location of a point on an object with respect to the camera coordinate system. Since origin of the image plane is located at the point $[f\ 0\ 0]^{\mathrm{T}}$ with respect to the camera frame, this object point would appear at a point x_p, y_p on the image plane. If the camera focal length is f, then perspective projection rules require that

$$\frac{x_p}{f} = \frac{y_c}{x_c} \quad (8)$$

$$\frac{y_p}{f} = \frac{z_c}{x_c}. \quad (9)$$

Now, if x_b, y_b, z_b are the position vector components of the point x_c, y_c, z_c in the body axis system,

$$\begin{bmatrix} x_c \\ y_c \\ z_c \end{bmatrix} = \mathbf{T}_1 \begin{bmatrix} x_b - l_1 \\ y_b - l_2 \\ z_b - l_3 \end{bmatrix} \quad (10)$$

where

$$\mathbf{T}_1 = \begin{bmatrix} c\epsilon_2 c\epsilon_1 & c\epsilon_2 s\epsilon_1 & -s\epsilon_2 \\ s\epsilon_3 s\epsilon_2 c\epsilon_1 - c\epsilon_3 s\epsilon_1 & s\epsilon_3 s\epsilon_2 s\epsilon_1 + c\epsilon_3 c\epsilon_1 & s\epsilon_3 c\epsilon_2 \\ c\epsilon_3 s\epsilon_2 c\epsilon_1 + s\epsilon_3 s\epsilon_1 & c\epsilon_3 s\epsilon_2 s\epsilon_1 - s\epsilon_3 c\epsilon_1 & c\epsilon_3 c\epsilon_2 \end{bmatrix}. \quad (11)$$

The variables c and s in the 3×3 matrix in (11) denote the sine and cosine functions. In a more concise notation,

$$\mathbf{x}_c = \mathbf{T}_1(\mathbf{x}_b - \mathbf{l}). \quad (12)$$

Next, if the location of the same object with respect to an inertial frame is x, y, z, and the vehicle is located at a point x_v, y_v, z_v with respect to this inertial

frame, the position components of the object point in the body frame are given by

$$\begin{bmatrix} x_b \\ y_b \\ z_b \end{bmatrix} = \mathbf{T}_2 \begin{bmatrix} x - x_v \\ y - y_v \\ z - z_v \end{bmatrix} \tag{13}$$

where

$$\mathbf{T}_2 = \begin{bmatrix} c\theta c\psi & c\theta s\psi & -s\theta \\ s\phi s\theta c\psi - c\phi s\psi & s\phi s\theta s\psi + c\phi c\psi & s\phi c\theta \\ c\phi s\theta c\psi + s\phi s\psi & c\phi s\theta s\psi - s\phi c\psi & c\phi c\theta \end{bmatrix}. \tag{14}$$

Here, ψ, θ, ϕ are the yaw, pitch, and roll attitudes of the rotorcraft. Equation (13) can be written in a compact form as

$$\mathbf{x}_b = \mathbf{T}_2(\mathbf{x} - \mathbf{x}_v). \tag{15}$$

Since the objective is to eliminate the disparity vector **d** in favor of the object position vector components, (8) and (9) can be used to examine the changes in x_p, y_p in response to the changes in the vehicle location by Δx_v, Δy_v, Δz_v. For the sake of clarity, this can be carried out in two steps. First consider the changes in x_p, y_p in response to changes in x_c, y_c, z_c. This can be accomplished by evaluating the expressions (8) and (9) with the camera referenced object location being defined as $x_c + \Delta x_c$, $y_c + \Delta y_c$, $z_c + \Delta z_c$. Using elementary algebraic operations it can be shown that

$$\Delta x_p = f\frac{\Delta y_c}{x_c + \Delta x_c} - x_p\frac{\Delta x_c}{x_c + \Delta x_c} \tag{16}$$

$$\Delta y_p = f\frac{\Delta z_c}{x_c + \Delta x_c} - y_p\frac{\Delta x_c}{x_c + \Delta x_c}. \tag{17}$$

These changes in the image frames are assumed to occur solely due to the motion of the rotorcraft. Next examine the changes in x_c, y_c, z_c due to the changes in vehicle position components x_v, y_v, z_v. Using the coordinate transformations discussed (12) and (15) one has that

$$\Delta\mathbf{x}_c = \mathbf{T}_1\Delta\mathbf{x}_b \tag{18}$$

$$\Delta\mathbf{x}_b = \Delta\mathbf{T}_2(\mathbf{x} - \mathbf{x}_v) - \mathbf{T}_2\Delta\mathbf{x}_v - \Delta\mathbf{T}_2\Delta\mathbf{x}_v. \tag{19}$$

The matrix $\Delta\mathbf{T}_2$ is the change in the transformation matrix relating the body frame and the inertial frame caused by the changes in the vehicle attitude. Note that (18) assumes that the *camera is fixed relative to the vehicle*. Equation (19) assumes that the *obstacles are fixed with respect to the inertial frame*. Next substituting (19) in (18) results in

$$\Delta\mathbf{x}_c = \mathbf{T}_1[\Delta\mathbf{T}_2(\mathbf{x} - \mathbf{x}_v) - (\mathbf{T}_2 + \Delta\mathbf{T}_2)\Delta\mathbf{x}_v]. \tag{20}$$

Using (12) and (15),

$$\mathbf{x} - \mathbf{x}_v = \mathbf{T}_2^{\mathrm{T}}[\mathbf{T}_1^{\mathrm{T}}\mathbf{x}_c + \mathbf{l}]. \tag{21}$$

Substituting (21) in (20) yields

$$\Delta\mathbf{x}_c = \mathbf{T}_1[\Delta\mathbf{T}_2\mathbf{T}_2^{\mathrm{T}}(\mathbf{T}_1^{\mathrm{T}}\mathbf{x}_c + \mathbf{l}) - (\mathbf{T}_2 + \Delta\mathbf{T}_2)\Delta\mathbf{x}_v]. \tag{22}$$

Finally, dividing expression (22) by x_c on both sides:

$$\begin{bmatrix} \Delta x_c/x_c \\ \Delta y_c/x_c \\ \Delta z_c/x_c \end{bmatrix} = \mathbf{T}_1\Delta\mathbf{T}_2\mathbf{T}_2^{\mathrm{T}}\mathbf{T}_1^{\mathrm{T}} \begin{bmatrix} 1 \\ x_p/f \\ y_p/f \end{bmatrix} + \mathbf{T}_1\Delta\mathbf{T}_2\mathbf{T}_2^{\mathrm{T}} \begin{bmatrix} l_1/x_c \\ l_2/x_c \\ l_3/x_c \end{bmatrix} - \mathbf{T}_1(\mathbf{T}_2 + \Delta\mathbf{T}_2) \begin{bmatrix} \Delta x_v/x_c \\ \Delta y_v/x_c \\ \Delta z_v/x_c \end{bmatrix}. \tag{23}$$

For the sake of brevity, (23) can be expressed in the form

$$\begin{bmatrix} \Delta x_c/x_c \\ \Delta y_c/x_c \\ \Delta z_c/x_c \end{bmatrix} = \begin{bmatrix} k_0 + k_3/x_c \\ k_1 + k_4/x_c \\ k_2 + k_5/x_c \end{bmatrix} \tag{24}$$

with parameters k_0, k_1, k_2, k_3, k_4, k_5 being computed using the operations indicated in (23). The rows of (24) can now be substituted in the expressions (16) and (17) to yield

$$\Delta x_p = \frac{fk_1 - x_pk_0 + (fk_4 - x_pk_3)/x_c}{1 + k_0 + k_3/x_c} \tag{25}$$

$$\Delta y_p = \frac{fk_2 - y_pk_0 + (fk_5 - y_pk_3)/x_c}{1 + k_0 + k_3/x_c}. \tag{26}$$

Note that the Δx_p, Δy_p are bilinear with respect to the inverse of the object position component x_c measured with respect to the camera coordinate system. Next, (25) and (26) may be substituted in the Taylor series approximation of the correspondence equation (6) to yield an equation that relates the vehicle-camera motion parameters with the image irradiance partial derivatives. In order to simplify the development, only a linear approximation is discussed here. The approach to include second-order terms is direct. From (6), the first-order Taylor series approximation of the correspondence hypothesis is

$$E_1 - E_2 = \tfrac{1}{2}\left[\frac{\partial E_1}{\partial x_p} + \frac{\partial E_2}{\partial x_p}\right]\Delta x_p + \tfrac{1}{2}\left[\frac{\partial E_1}{\partial y_p} + \frac{\partial E_2}{\partial y_p}\right]\Delta y_p. \tag{27}$$

Substituting for the disparity components Δx_p, Δy_p in (27) from (25), (26) yields

$$x_c = \frac{k_3c_1 - a_1(fk_4 - x_pk_3) - b_1(fk_5 - y_pk_3)}{a_1(fk_1 - x_pk_0) + b_1(fk_2 - y_pk_0) - c_1(1 + k_0)} \tag{28}$$

where

$$a_1 = \frac{1}{2}\left[\frac{\partial E_1}{\partial x_p} + \frac{\partial E_2}{\partial x_p}\right] \tag{29}$$

$$b_1 = \frac{1}{2}\left[\frac{\partial E_1}{\partial y_p} + \frac{\partial E_2}{\partial y_p}\right] \tag{30}$$

$$c_1 = E_2 - E_1. \tag{31}$$

Various quantities on the right-hand side of (28) can be obtained from on-board instruments and the given image sequences. Hence, (28) can be solved to obtain x_c. Once x_c is computed at every pixel location, the two remaining components of the object position vector at every pixel can be determined using the relations:

$$y_c = x_c x_p / f, \qquad z_c = x_c y_p / f. \tag{32}$$

The position of the object with respect to the inertial frame is then given by

$$\mathbf{x} = \mathbf{x}_v + \mathbf{T}_2^{\mathrm{T}}(\mathbf{T}_1^{\mathrm{T}}\mathbf{x}_c + \mathbf{l}). \tag{33}$$

The instantaneous vehicle position vector x_v, the instantaneous transformation matrix from the vehicle body frame to the inertial frame $\mathbf{T}_2$, its change $\Delta\mathbf{T}_2$, the constant transformation matrix from the vehicle body frame to the camera frame $\mathbf{T}_1$, the camera focal length f and its orientation angles are known from various on-board instruments. Hence, the object location can be calculated using expression (33).

The image sequence related quantities in (28) are the image spatial partial derivatives $\partial E_1/\partial x_p$, $\partial E_1/\partial y_p$, $\partial E_2/\partial x_p$, $\partial E_2/\partial y_p$ and the irradiance difference $E_2 - E_1$ at every pixel. A method for estimating these quantities is presented in the next section.

PARTIAL DERIVATIVE ESTIMATION

Several numerical techniques are available in the literature for the computation of the partial derivatives [10]. These range from simple central difference schemes to very sophisticated algorithms that reject noise and unwanted frequency components in the input signal. It is well known in the signal processing literature that derivative estimation is a noise amplifying process. Given an irradiance distribution $E(x_p, y_p)$, the objective of the partial derivative estimators is to provide relatively noise-free estimates of $\partial E/\partial x_p$, $\partial E/\partial y_p$, $\partial^2 E/\partial x_p^2$, $\partial^2 E/\partial y_p^2$, $\partial^2 E/\partial x_p \partial y_p, \ldots$, together with a consistent image irradiance distribution. Additionally, it is desirable to carry out this estimation process as fast as possible to enable real-time or near real-time implementation of the object location algorithm.

Frequency domain estimation methods are popular in the image processing literature [10]. While these approaches enable a direct formulation of the noncasual estimation problem, they are unattractive for use with electro-optical sensors that form images using a sequential scanning process. In the following, a partial derivative estimator is formulated directly in the spatial domain. Unlike the frequency domain estimators, the present formulation employs causal estimators to permit sequential computations. Although this approximation compromises accuracy to a certain extent, numerical experiments have shown that the error magnitude can be controlled by a careful selection of the estimator parameters.

Following the frequency domain image processing methods [10], the image irradiance distribution $E(x_p, y_p)$ is assumed to be factored into a product of two functions of one variable each, denoted by the symbols $e_1(x_p)$ and $e_2(y_p)$. This factorization allows the evaluation of double integrals as products of two, single integrals. Note that such a factorization is routinely employed to produce solutions of linear partial differential equations [11]. In the following, estimated quantities are denoted by a $\hat{}$. Thus,

$$E = e_1(x_p)e_2(y_p), \qquad \hat{E} = \hat{e}_1(x_p)\hat{e}_2(y_p) \tag{34}$$

$\hat{E}$ is the estimated irradiance distribution. The partial derivatives of $\hat{E}$ can be written in terms of the total derivatives of its factors $\hat{e}_1$, $\hat{e}_2$ as

$$\frac{\partial \hat{E}}{\partial x_p} = \hat{e}_2 \frac{d\hat{e}_1}{dx_p}, \qquad \frac{\partial \hat{E}}{\partial y_p} = \hat{e}_1 \frac{d\hat{e}_2}{dy_p}$$

$$\frac{\partial^2 \hat{E}}{\partial x_p^2} = \hat{e}_2 \frac{d^2\hat{e}_1}{dx_p^2}, \qquad \frac{\partial^2 \hat{E}}{\partial y_p^2} = \hat{e}_1 \frac{d^2\hat{e}_2}{dy_p^2}$$

$$\frac{\partial^2 \hat{E}}{\partial x_p \partial y_p} = \frac{d\hat{e}_1}{dx_p}\frac{d\hat{e}_2}{dy_p}, \ldots . \tag{35}$$

With this factorization, the estimation problem can be cast as two, coupled, one-dimensional estimation problems. Although the estimation problem can be formulated either as a serial process or as a parallel process [9], a serial implementation is discussed here.

Define $\mathbf{p}$ as the n-dimensional estimator state vector. The estimator dimension n may be selected based on the order of partial derivatives to be estimated and the desired smoothness requirement. For instance, if it is desired to estimate the first-order and the second-order partial derivatives with the requirement that the second-order partial derivatives be smooth, n has to be at least 3. Next consider a linear dynamic process evolving along the x_p direction with the measured image irradiance E as the input.

$$\frac{d}{dx_p}\mathbf{p} = \mathbf{A}\mathbf{p} + \mathbf{B}E. \tag{36}$$

This dynamic process is assumed to evolve along the image scan lines. The matrices $\mathbf{A}$ and $\mathbf{B}$ can be chosen to obtain the desired transmission gain and bandwidth for the x_p spatial frequencies. The output

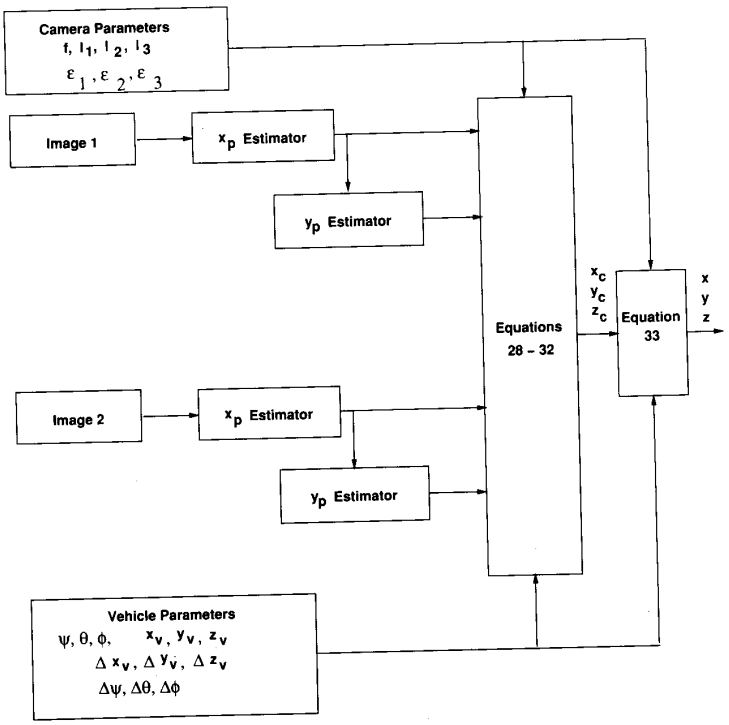

Fig. 2. Electro-optical navigation algorithm.

equation for this linear dynamic process can be defined as

$$\mathbf{r} = \mathbf{C}\mathbf{p} + \mathbf{D}E, \quad \mathbf{r} = e_2 \left[\hat{e}_1 \frac{d\hat{e}_1}{dx_p} \frac{d^2\hat{e}_1}{dx_p^2} \cdots \right]^{\mathrm{T}}. \tag{37}$$

The matrices **C**, **D** should be chosen based on the linear dynamic system (36) dimension and on the desired orders of the partial derivatives.

Similarly, define a linear dynamic process evolving along the y_p direction, with the first element of the vector **r** as the input, i.e.,

$$\frac{d}{dy_p}\mathbf{q} = \mathbf{M}\mathbf{q} + \mathbf{N}e_2\hat{e}_1. \tag{38}$$

The matrices **M** and **N** can be chosen to obtain the desired gain and bandwidth for the y_p spatial frequency components. The output equation of this dynamic process can be chosen as

$$\mathbf{s} = \mathbf{K}\mathbf{q} + \mathbf{L}\hat{e}_1 e_2,$$
$$\mathbf{s} = \hat{e}_1 \left[\hat{e}_2 \frac{d\hat{e}_2}{dy_p} \frac{d^2\hat{e}_2}{dy_p^2} \cdots \right]^{\mathrm{T}} \tag{39}$$

with the matrices **K**, **L** being chosen in the same manner as the output matrices **C**, **D** in (37). The vectors **r** and **s** can now be used to compute the estimated image irradiance and its various partial derivatives. Elements of these vectors are denoted by lower case letters in the following. It can be verified that

$$\hat{E} = s_1, \quad \frac{\partial \hat{E}}{\partial x_p} = \frac{s_1 r_2}{r_1}, \quad \frac{\partial \hat{E}}{\partial y_p} = s_2,$$
$$\frac{\partial^2 \hat{E}}{\partial x_p^2} = \frac{s_1 r_3}{r_1}, \quad \frac{\partial^2 \hat{E}}{\partial y_p^2} = s_3 \tag{40}$$
$$\frac{\partial^2 \hat{E}}{\partial x_p \partial y_p} = \frac{r_2 s_2}{r_1}.$$

In (40), it is important to ensure that the first element of the **r** vector r_1 does not become zero at any point on the image. This can be assured by adding a constant bias to the input image E and subtracting this bias at the output. Note that such an operation does not alter the partial derivative estimates.

Since the partial derivative estimation process was formulated keeping the image forming process in view, these quantities are available as the image is being formed. As a result, by the time the image scanning process is complete, various parameters required in (28) can be computed. Thus, after the availability of the first frame, the object location computations can be completed at the camera frame rate.

A block diagram of the object location algorithm is given in Fig. 2. This block diagram assumes that an image pair is available at the beginning of the computations. The estimators along the X_p and Y_p directions provide the noise-attenuated partial

Fig. 3. First sample image.

Fig. 4. Second sample image.

derivatives together with consistent image irradiance estimates. The coefficients of (28) are then computed by combining this information with the vehicle-camera motion data. The position vector component x_c corresponding to every point on the image plane is then computed by applying (28) at every pixel. The vehicle and the camera rotational and translational data required for this calculation are assumed to be available from on-board instruments. The other components of the position vector y_c, z_c at every pixel are then determined using (32).

The quantities x_c, y_c, z_c are computed only at regions where the inter-frame irradiance changes and the spatial partial derivatives are sufficiently large. The remaining points are assigned a predefined maximum scene depth. Once the position vectors in the camera frame become available, the expression (33) can be used to transform the position components into the inertial frame.

RESULTS AND DISCUSSIONS

The performance of the obstacle location algorithm was tested using two different image sequences. The first of these was a laboratory scene used in [8 and 9]. The second test image sequence was obtained from a camera mounted on the nose of a helicopter. Results obtained using the second image sequence are discussed here. Two images from an airborne camera are shown in Figs. 3 and 4. The camera was mounted on the nose of a fully instrumented CH-47B Chinook helicopter. The cameras were calibrated using a calibration grid and a transit, and laser distance measuring equipment [12]. The images were recorded on a conventional video cassette recorder. These images were later digitized. The digital images consist of a 512×512 pixel arrays, with 8 bit gray-scale digitization. The camera was operating at a rate of 30 frames/s. During the imaging process, the rotorcraft was flying at an altitude of about 12 ft above the runway at a speed of 32.6 ft/s. The image pair given in Figs. 3 and 4 are temporally separated by 0.17 s. During this time, the rotorcraft underwent a translational motion of $[5.41, -0.44, 0.02]^T$ ft and experienced an attitude motion of 0.059 deg about the pitch axis, -0.08 deg about the yaw axis, and 0.12 deg about the roll axis.

Besides other details, Figs. 3 and 4 show a runway, and five vehicles parked on the two sides. The instrumented nose boom of the helicopter is clearly visible at the top right-hand part of the image. Time synchronization parameters identifying this frame are displayed in a subpicture on the top left-hand side of the image.

As indicated elsewhere in this paper, the ranging algorithm requires the spatial derivatives of the image irradiance. These spatial partial derivatives together with consistent image irradiance distributions were computed using irradiance estimators of the form:

$$\frac{dp}{dx_p} = -5.0p + 5.0E$$
$$\begin{bmatrix} r_1 \\ r_2 \end{bmatrix} = \begin{bmatrix} 1 \\ -5.0 \end{bmatrix} p + \begin{bmatrix} 0 \\ 5.0 \end{bmatrix} E \tag{41}$$

$$\frac{dq}{dy_p} = -5.0p + 5.0\hat{e}_1 e_2$$
$$\begin{bmatrix} s_1 \\ s_2 \end{bmatrix} = \begin{bmatrix} 1 \\ -5.0 \end{bmatrix} q + \begin{bmatrix} 0 \\ 5.0 \end{bmatrix} \hat{e}_1 e_2. \tag{42}$$

Output of these estimators were used in (40) to form the various partial derivatives. These values were then used together with the vehicle motion data obtained from the on-board inertial navigation system to compute the distance to various obstacles. Since the range calculations given in this initial study were carried out using the leading term of the Taylor series expansion (6), first-order estimators were adequate.

The object location data was computed at 480 points on the image plane. In Fig. 5, the points at which the location data was computed are shown as white dots. This represents about 0.2% of the possible

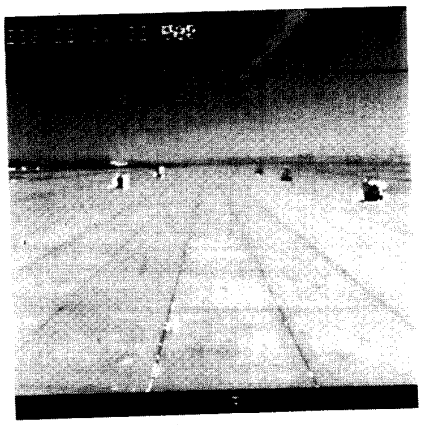

Fig. 5. Points at which object location data are computed.

TABLE I
Comparison Between Actual Range (Feet) And Estimated Range (Feet) For Some Objects In The Scene

Object	Actual Range	Estimated Range	Number of Points
Vehicle 1	356.4	335.6	113
Vehicle 2	607.0	395.9	24
Vehicle 3	232.8	202.1	160

262,144 points. The object location data can be reliably recovered only at those points where a significant image intensity change is detected between the image frames.

Table I summarizes the comparison between computed and actual locations of some of the objects in this scene. This table also gives the number of points at which the computations were carried out for each object. Even though the image was not of high quality, note that the algorithm determines the location of two vehicles with acceptable accuracy. There is a large error in the location of the vehicle number 2. At this stage it appears that this inaccuracy may be caused by the low resolution of the image. Additional tests are currently being carried out to determine the image resolution requirements for obtaining a desired position determination accuracy.

CONCLUSIONS

A passive image-based obstacle location algorithm for use in the guidance of rotorcraft during low altitude flight was described. The algorithm uses the vehicle-camera translation and rotational motion data together with the image sequences to compute the location of various objects within the field-of-view.

The method uses a Taylor series approximation of the correspondence hypothesis together with the perspective projection geometry. The present research generalizes previous work on an object location algorithm to include both the translational and rotational motion of the imaging devices and the vehicle. The resulting algorithm is more general and can operate in multicamera imaging environments. The performance results using an image sequence from an airborne camera are given.

REFERENCES

[1] Cheng, V. H. L., and Sridhar, B. (1991)
Considerations for automated nap-of-the-earth rotorcraft flight.
Journal of the American Helicopter Society, **36**, 2 (Apr. 1991), 61–69.

[2] Cheng, V. H. L. (1990)
Concept development of automatic guidance for rotorcraft obstacle avoidance.
IEEE Transactions on Robotics and Automation, **6**, 2 (Apr. 1990), 252–257.

[3] Menon, P. K. A., Chatterji, G. B., and Sridhar, B. (1991)
Vision-based optimal obstacle-avoidance guidance for rotorcraft.
Presented at the AIAA Guidance, Navigation, and Control Conference, New Orleans, LA, Aug. 12–14, 1991.

[4] Sridhar, B., Suorsa, R., and Hussien, B. (1992)
Passive range estimation for rotorcraft low altitude flight.
Technical Memo 103897, NASA, 1992. Accepted for publicaion in *Machine Vision and Applications*, 1992.

[5] Negahdaripour, S., and Horn, B. K. P. (1987)
Direct passive navigation.
IEEE Transactions on Pattern Analysis and Machine Intelligence, **PAMI-9** (Jan. 1987), 168–176.

[6] Skifstad, K., and Jain, R. (1989)
Range estimation from intensity gradient analysis.
Machine Vision and Applications, **2**, (1989), 81–102.

[7] Menon, P. K. A., and Sridhar, B. (1989)
Passive navigation using image irradiance tracking.
Presented at the AIAA Guidance, Navigation, and Control Conference, Boston, MA, Aug. 14–16, 1989.

[8] Menon, P. K. A., and Sridhar, B. (1990)
Image-based range determination.
Presented at the AIAA Guidance, Navigation, and Control Conference, Portland, OR, Aug. 14–16, 1990. Accepted for publication in *Journal of Guidance, Control, and Dynamics*, 1991.

[9] Menon, P. K. A., Chatterji, G. B., and Sridhar, B. (1991)
A fast algorithm for image-based ranging.
Presented at the SPIE International Symposium on Optical Engineering and Photonics in Aerospace Sensing, Orlando, FL, Apr. 1–5, 1991.

[10] Horn, B. K. P. (1986)
Robot Vision.
New York: McGraw Hill, 1986.

[11] Pipes, L. A. (1958)
Applied Mathematics for Engineers and Physicists.
New York: McGraw Hill, 1958.

[12] Smith, P. N. (1990)
Flight data acquisition methodology for validation of passive ranging algorithms for obstacle avoidance.
Technical Memo NASA, 102809, Ames Research Center, Moffett Field, CA, Oct. 1990.

P. K. A. Menon received a Ph.D. degree in aerospace engineering from Virginia Polytechnic Institute, Blacksburg, in 1983, an M.E. degree in aeronautical engineering from the Indian Institute of Science, Bangalore, India, in 1975, and a B.E. degree in mechanical engineering from Osmania University in 1973.

He is currently the president of Optimal Synthesis, a high technology company. Previously, he was an Associate Professor in the School of Aerospace Engineering, Georgia Institute of Technology, Atlanta. He spent three years as a visiting scientist with the FSN Branch, NASA Ames Research Center, Moffet Field, CA, working on navigation and guidance schemes for rotorcraft and high performance aircraft. Since January 1989, he has also been an adjunct faculty member at Santa Clara University, Santa Clara, CA. During 1983–1986 Dr. Menon was with the Integrated Systems, Inc. where he was involved in the development of advanced guidance laws and flight control systems for missiles and aircraft. Dr. Menon was a research scientist with the Indian Space Research Organization from 1976 to 1981, where he conducted research on dynamics and control of launch vehicles, hybrid computer simulation and postflight data analysis techniques.

Dr. Menon is an Associate Fellow of the American Institute of Aeronautics and Astronautics, Sigma Gamma Tau and Sigma Xi. He is an Associate Editor of the *Journal of Guidance, Control, and Dynamics*. He has presented over 60 papers at various conferences and has contributed over 30 journal papers.

Gano B. Chatterji received the degree of Bachelor of Technology in mechanical engineering from the Indian Institute of Technology, Kanpur, India. He received the degree of Master of Science in engineering science from the University of Mississippi.

From 1985 to 1990, Mr. Chatterji was employed by Integrated Systems, Inc. Since 1990, Mr. Chatterji has been at the FSN branch of NASA Ames Research Center as an employee of Sterling Software. His interests are in optimal control, guidance, navigation, optimization, mathematical modeling of systems, systems integration, and computer vision.

Banavar Sridhar (S'68—M'73—SM'91) received the B.E. degree in electrical engineering from the Indian Institute of Science, Bangalore, India, and the M.S. and Ph.D. degrees in electrical engineering from the University of Connecticut, Storrs.

From 1973 to 1976, he held a National Research Council Fellowship at NASA Ames Research Center, Moffett Field, CA. He worked at Systems Control, Inc., Palo Alto, CA and Lockheed Palo Alto Research Center before joining NASA Ames Research Center in 1986. His research interests are in the application of control and computer vision techniques to autonomous systems.

Dr. Sridhar served as Chairman of the Santa Clara Valley Chapter, IEEE Control Systems/Cybernetics Society for the period 1982–1985. Dr. Sridhar was an Associate Editor of the *IEEE Transactions on Automatic Control* and is an Associate Editor of the *IEEE Control Systems Magazine*. During 1991, Dr. Sridhar received the "Engineer of the Year" award from the Bay Area Section of the American Institute of Aeronautics and Astronautics.